PHYSICAL REVIEW E **96**, 050601(R) (2017)

Discontinuous fluidization transition in time-correlated assemblies of actively deforming particles

Elsen Tjhung[1,2] and Ludovic Berthier[1]

[1]*Laboratoire Charles Coulomb, UMR 5221, CNRS and Université Montpellier, 34095 Montpellier, France*

[2]*Department of Applied Mathematics and Theoretical Physics, University of Cambridge, Cambridge CB3 0WA, United Kingdom*

(Received 11 August 2016; revised manuscript received 25 September 2017; published 22 November 2017)

Tracking experiments in dense biological tissues reveal a diversity of sources for local energy injection at the cell scale. The effect of cell motility has been largely studied, but much less is known about the effect of the observed volume fluctuations of individual cells. We consider a microscopic model of "actively deforming" particles where local fluctuations of the particle size constitute a unique source of motion. We demonstrate that collective motion can emerge under the sole influence of such active volume fluctuations. We interpret the onset of diffusive motion as a nonequilibrium first-order phase transition, which arises at a well-defined amplitude of self-deformation. This behavior contrasts with the glassy dynamics produced by self-propulsion, but resembles the mechanical response of soft solids under mechanical deformation. It thus constitutes an example of an active yielding transition.

DOI: 10.1103/PhysRevE.96.050601

Active matter represents a class of nonequilibrium systems that is currently under intense scrutiny [1,2]. In contrast to externally driven systems (such as sheared materials), active matter is driven out of equilibrium at the scale of its microscopic constituents. Well-studied examples include biological tissues [3], bacterial suspensions [4], and active granular and colloidal particles [5–8].

Epithelial tissues constitute a biologically relevant active system composed of densely packed eukaryotic cells [3,9–14]. Such tissues display a surprisingly fast and collective dynamics, which would not take place under equilibrium conditions [10]. This dynamics has been ascribed to at least three distinct active processes [13]: (i) self-propulsion through cell motility such as crawling [15], (ii) self-deformation through protrusion and contraction [16–18], and (iii) cell division and apoptosis [14]. The vertex model for tissues [12,19,20] includes the first two of these active processes and predicts a continuous static transition from an arrested to a flowing state [21]. Another theoretical line of research is based on self-propelled particles [22] which display at high density a nonequilibrium glass transition [23,24] accompanied by a continuous increase of space and time correlations which diverge on approaching the arrested phase [25–27]. However, typical correlation length scales in tissues do not seem to diverge [9,11,28,29].

To disentangle the dynamic consequences of the various sources of activity in tissues at large scale, we suggest to decompose the original complex problem into simpler ones, and to study particle-based models which only include a single specific source of activity. This strategy was followed earlier for self-propulsion, but experiments are instead often modeled by complex models with many competing processes [18,29,30]. We argue that it is relevant to introduce also simplified models to analyze the effect of active particle deformation in a dense assembly of nonpropelled soft objects. Specifically, we model a dense system that is driven out of equilibrium locally through "self-deformation" rather than self-propulsion. We study soft particles that actively change their size, while energy is being dissipated through viscous damping. As a starting point, we consider the simplest form of self-deformation, in which the diameter of each spherical particle oscillates at very low frequency, in a way that is directly inspired by experimental observations in real tissues [16]. The interest of such modeling is that activity is thus controlled by a unique adimensional parameter, a, which quantifies the relative change of the particle diameter within a deformation period. Our aim is not to propose a realistic model of a tissue, but rather to answer a more fundamental physical question regarding the role of active volume fluctuations in tissue dynamics. Despite its relevance, such a class of models has, to our knowledge, not been analyzed before in a statistical mechanics context.

First we consider the case when each particle's diameter oscillates with the same frequency ω, where $1/\omega$ is assumed to be much longer than the microscopic dissipation time scale of the system. Our main result is the existence of a discontinuous nonequilibrium phase transition from an arrested disordered solid to a flowing fluid state at some critical activity, a_c, with no diverging time scales or length scales. In particular, we observe a modest increase of one order of magnitude in the relaxation times of the fluid before the system gets discontinuously trapped in an arrested phase at $a = a_c$. Our system also shows a strong hysteresis as seen in equilibrium first-order phase transitions. This scenario for the fluidization transition differs markedly from that of self-propelled particles in which a dramatic continuous slowing down is observed [24–27]. We propose that the correct analogy for our observations is not with a glass [24] or jamming [23] transition, but rather with the yielding transition of amorphous solids [31], which start flowing irreversibly when mechanically perturbed beyond a force threshold, the yield stress. Therefore, actively deforming particles undergo an "active yielding transition," which represents a novel paradigm for the collective motion of active materials.

Finally, we also consider the case when each particle deforms with a different frequency (see Sec. I in the Supplemental Material (SM) [32]). In this case, the discontinuous transition remains robust as long as the width of the frequency spectrum is narrow enough. Then we also consider the case when each particle oscillates with a given distribution of frequencies $P(\omega)$ (see Sec. II in the SM). In this case, we show the discontinuous transition still remains robust. Lastly, we consider the case

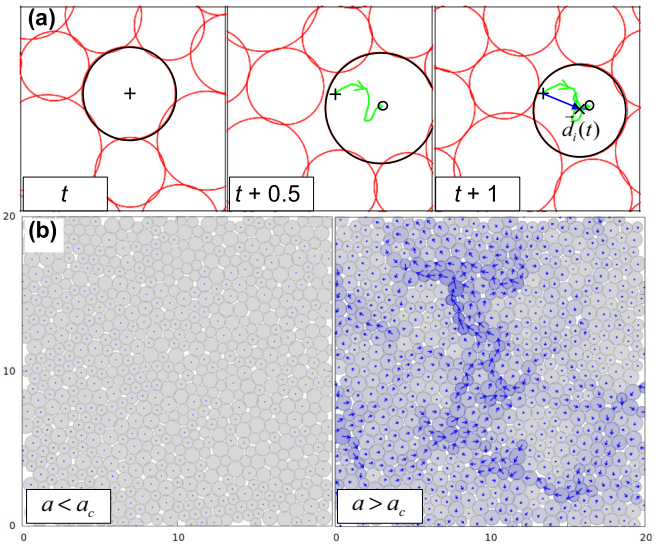

FIG. 1. (a) Snapshots of the system over one cycle of active deformation. The green curve is the trajectory of the highlighted particle during one cycle. The blue arrow represents its displacement after one cycle $\vec{d}_i(t) = \vec{r}_i(t+1) - \vec{r}_i(t)$. (b) One-cycle displacement map $\vec{d}_i(t)$ in steady state for the disordered solid phase ($a = 0.047 < a_c \approx 0.049$, left) and in the fluid phase ($a = 0.051 > a_c$, right). In the solid phase, particles approximately return to their position after each cycle. In the fluid, there are regions of large displacements where irreversible rearrangements take place. The transition between reversible and irreversible phases at a_c is discontinuous.

when each particle oscillates with a random but time-correlated noise (Ornstein-Uhlenbeck noise; Sec. III in the SM). In this case, the transition becomes a nonequilibrium glass transition with continuously diverging time and length scales. This is perhaps unsurprising, because the physics becomes similar to that of self-propelled particles where the active forces are characterized by finite persistence times. Overall, these results strengthen our hypothesis for the active yielding transition.

We consider a dense suspension of N soft circular particles at zero temperature in a two-dimensional square box of linear size L with periodic boundary conditions. The interaction between the particles is modeled by a short-ranged repulsive harmonic potential, similar to jammed foams [33]: $V(r_{ij}) = \frac{\epsilon}{2}(1 - r_{ij}/\sigma_{ij})^2 H(\sigma_{ij} - r_{ij})$, where $r_{ij} = |\vec{r}_i - \vec{r}_j|$, $\sigma_{ij} = (\sigma_i + \sigma_j)/2$, with σ_i and $\vec{r}_i$ the diameter and position of particle i, respectively. The energy scale of the repulsive force is set by ϵ, and $H(x)$ is the heaviside function, defined such that $H(x \geqslant 0) = 1$. In the overdamped limit, the dynamics of each particle is described by a Langevin equation:

$$\xi \frac{d\vec{r}_i}{dt} = -\sum_{j \neq i} \frac{\partial V(r_{ij})}{\partial \vec{r}_j}, \tag{1}$$

where ξ is a friction coefficient. The dissipation time scale is $\tau_0 = \xi \sigma_0^2/\epsilon$, where σ_0 sets the particle diameter (see below). Physically, τ_0 is the typical time scale for a system described by Eq. (1) to come at rest without forcing.

We drive the system out of equilibrium by oscillating the diameter of each particle around its mean value σ_i^0, as shown in Fig. 1(a):

$$\sigma_i(t) = \sigma_i^0[1 + a\ \cos(\omega t + \psi_i)], \tag{2}$$

where $T = 2\pi/\omega$ is the period of oscillation which we use as our time unit, and a is an adimensional parameter which quantifies the intensity of the activity. We impose very slow oscillations, $T \gg \tau_0$, such that the system is always located near an energy minimum and inertial and hydrodynamic effects can be neglected. Specifically, we use $T = 820\tau_0$. The average diameters σ_i^0 are drawn from a bidisperse distribution of diameters $0.71\sigma_0$ and σ_0 with 3:2 proportion, in order to prevent crystallization. We use σ_0 as unit length. We have introduced in Eq. (2) a random phase ψ_i for each particle to constrain the total area fraction $\phi = \sum_i \frac{\pi \sigma_i^2(t)}{4L^2}$ to be strictly constant in time. The case with $\psi_i \equiv 0$ would correspond to affine compressions and expansions, which would then amount to studying the rheological response of the jammed solid forced at large scale, not an active material forced locally. We consider jammed systems with $\phi = 0.94$, as appropriate for confluent tissues. Most simulations were performed with a very large system of $N = 16\,000$ particles (typically $L \approx 100\sigma_0$). We converged to this large value using simulations with increasing sizes, seeking the disappearance of finite-size effects. We also use finite-size scaling analysis to locate the phase transition with greater accuracy. For each a value, we prepare fully random systems and apply the periodic perturbation until the system has reached steady state, either arrested or flowing. We then perform steady-state measurements using averaging over time and initial conditions (in the flowing phase), or over initial conditions (in the arrested phase).

Figure 1(a) highlights the trajectory of a particle during one period. We define the one-cycle displacement, $\vec{d}_i(t) = \vec{r}_i(t+1) - \vec{r}_i(t)$, as shown in Fig. 1(a). Collecting the displacement of all particles we obtain the steady-state one-cycle displacement map shown in Fig. 1(b) for both arrested and flowing phases. In the arrested phase, displacements are all very small and particles approximately return to the same position after each cycle, without undergoing configurational change. On the other hand, at large activity we observe regions of very large displacements where irreversible particle rearrangements occur within one cycle. These local plastic events are spatially disordered, and they coexist with regions where displacements are smaller: the dynamics is spatially heterogeneous. Clearly, Fig. 1 indicates the existence of an arrested phase where particles do not move for small a, and of a flowing phase for large a where irreversible rearrangements take place during each cycle. In the following we demonstrate that the transition between these two regimes occurs at a well-defined activity value, a_c, and that it corresponds to a first-order phase transition.

We start by showing in Fig. 2(a) the probability distribution of one-cycle displacements, $P(\delta x_i)$, where $\delta x_i = |x_i(t+1) - x_i(t)|$ (we use isotropy and average over x and y directions). In the flowing phase ($a > a_c \simeq 0.049$), $P(\delta x_i)$ has a broad, nearly exponential tail, stemming from particles involved in local rearrangements (or localized particle's motions whose displacements are larger than the diameter). As a result, all particles move significantly during each cycle. As shown below, the accumulation of these local plastic events over many

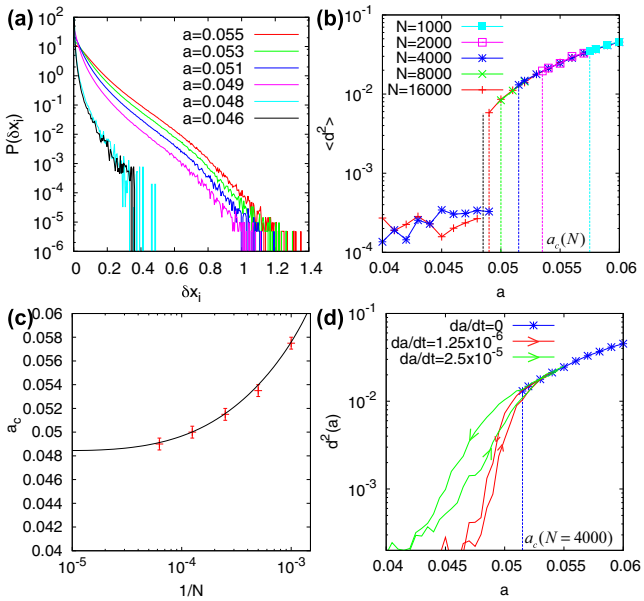

FIG. 2. (a) Probability distribution of the one-cycle particle displacements $P(\delta x_i)$ for different activities a. The distribution changes discontinuously between flowing ($a > a_c \simeq 0.049$) and arrested ($a < a_c$) phases. (b) Averaged one-cycle displacement squared at steady state for different system sizes N. $\langle d^2 \rangle$ is large above a_c, and drops discontinuously to nearly zero below a_c. The black vertical line represents $a_c(N \to \infty)$. (c) The critical activity $a_c(N)$ tends to a finite value $\simeq 0.049$ as $1/N \to 0$. (d) Evolution of $\langle d^2 \rangle$ for $N = 4000$ as the activity is cycled at finite rate between $a = a_1 > a_c$ and $a = a_2 < a_c$. The blue curve represents the steady-state value. The hysteretic response gets sharper as $\frac{da}{dt}$ decreases.

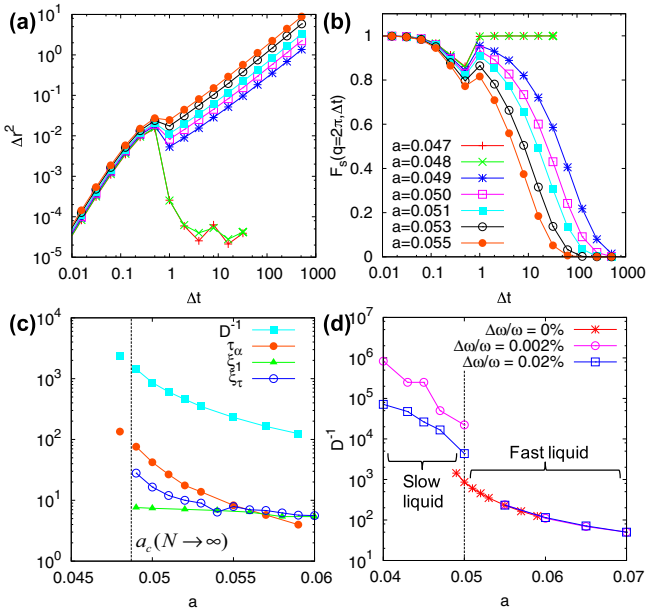

FIG. 3. (a) Mean-squared displacements are diffusive for $a > a_c$, but remain localized for $a < a_c$, with a sharp discontinuity at a_c. (b) A similar discontinuous behavior is observed for the self-intermediate scattering function $F_s(q, \Delta t)$, which decays rapidly to 0 above a_c, but does not decay below a_c. (c) shows the typical time scales (D^{-1} and τ) and dynamic length scales (ξ_1 and ξ_τ), which only increase modestly by about 1 decade as $a \to a_c^+$. Below a_c we find a metastable flowing phase where D^{-1} and τ can be measured (isolated points) before the system fully arrests. (d) shows the inverse diffusion constant D^{-1} as a function of activity a when a finite frequency bandwidth $\Delta\omega/\omega$ is introduced, showing that the arrested phase is now characterized by a very low diffusivity.

cycles gives rise to diffusive behavior and structural relaxation at large times. On the other hand, in the solid phase ($a < a_c$), the exponential tail in $P(\delta x_i)$ disappears and is replaced by a narrow distribution characterized by an average displacement per cycle that is considerably smaller. We show below that these small displacements do not produce diffusive but only localized dynamics.

Crucially, the behavior of $P(\delta x_i)$ changes abruptly when a crosses a_c. We quantify this observation using a dynamic order parameter for this phase change: $\langle d^2 \rangle = \langle |\vec{d}_i(t)|^2 \rangle$, where the brackets represent an average over time and particles in steady state. (To check if the system has reached a steady state, we measure the averaged one-cycle displacement squared $\sum_i |\vec{d}_i(t)|^2$ as a function of simulation time t.) A similar quantity was defined in the context of the yielding transition in oscillatory shear [34,35]. In Fig. 2(b), we plot $\langle d^2 \rangle$ as a function of activity for different system sizes. The flowing phase is characterized by large particle displacements with $\langle d^2 \rangle \gtrsim 0.01$, whereas in the arrested phase, $\langle d^2 \rangle$ is about 20 times smaller. Furthermore, $\langle d^2 \rangle$ jumps discontinuously at a well-defined critical activity, $a_c(N)$. To determine $a_c(N)$ we perform eight independent simulations from different initial configurations at each activity. We define a_c such that the eight runs remain diffusive for $a > a_c$ after a large time, $t = 10^4$. In addition to the sharpness of the phase change, we also observe finite-size effects, since $a_c(N)$ decreases weakly with N. As shown in Fig. 2(c), when plotted against $1/N$, it is clear that a_c extrapolates to a finite value $a_c \approx 0.049$ when $N \to \infty$.

We substantiate further the discontinuous nature of the transition by studying hysteresis effects. In Fig. 2(d), we measure how $\langle d^2 \rangle$ changes as we slowly cycle the activity $a(t)$ between $a = a_1 > a_c$ and $a = a_2 < a_c$ at a constant rate $\frac{da}{dt}$. We obtain the evolution for $\langle d^2 \rangle$ by averaging over 10^3 such cycles. We observe hysteresis cycles that become sharper and narrower as the sweeping rate becomes slower. Such phenomenology is again representative of first-order phase transitions.

We now turn to the long-time dynamics and measure the mean-squared displacement (MSD) at steady state: $\Delta r^2(\Delta t) = \langle |\vec{r}_i(\Delta t) - \vec{r}_i(0)|^2 \rangle$ [see Fig. 3(a)] . In the flowing phase ($a > a_c$), the system becomes diffusive at long times $\Delta r^2(\Delta t \to \infty) \approx 4D\Delta t$, which defines the diffusion constant D. In the arrested phase instead, the MSD saturates to a small, finite value at long times, demonstrating particle localization in this regime. As a result, we find that $D > 0$ above a_c and $D = 0$ below, with an abrupt change at a_c, as shown in Fig. 3(c). This sharp change in the long-time dynamics is also detected using the intermediate scattering function: $F_s(q, \Delta t) = \langle e^{i\vec{q}\cdot[\vec{r}_i(\Delta t) - \vec{r}_i(0)]} \rangle$, which decays from 1 to 0 when particles move on average a distance $2\pi/|\vec{q}|$. In Fig. 3(b), we show the time decay of $F_s(q, \Delta t)$ for $q = 2\pi$, which

corresponds to particles diffusing over a distance comparable to their diameter. Above a_c, $F_s(q,\Delta t)$ decays to 0 relatively rapidly. We extract a relaxation time τ as $F_s(q,\tau) = 1/e$, with again a discontinuous change between the two phases. We extract a relaxation time τ as $F_s(q,\tau) = 1/e$, and so $\tau = \infty$ below a_c.

In Fig. 3(c) we report D^{-1} and τ as a function of activity a. Both measures of long-time dynamics increase modestly by about 1 decade as $a \to a_c^+$, and they do not diverge. In addition, just below a_c, we find that the flowing phase can be "metastable" for a long time of order 30τ before suddenly evolving toward the arrested phase. Within this metastability window, long-time dynamical properties can be measured and we plot D^{-1} and τ for this metastable liquid phase as isolated points in Fig. 3(c), which appear as the continuation of data at $a > a_c$. These observations confirm that both time scales do not diverge at a_c and illustrate the first-order nature of the phase transition at a_c.

In Fig. 3(c), we also plot two dynamic correlation length scales measured in the flowing phase which only increase modestly without divergence at a_c. These dynamic length scales are obtained from analysis of a four-point dynamic structure (see [36] for details about this classic measure of spatially heterogeneous dynamics). In particular, we have studied dynamic correlations both over a delay time $\Delta t = 1$ to probe spatial correlations of the one-cycle displacement map [see Fig. 1(b)], which gives us the one-cycle correlation length ξ_1. We also measured the dynamic length scale ξ_τ characterizing the long-time dynamics by setting $\Delta t = \tau$. Both length scales increase modestly as $a \to a_c^+$, revealing collective motion in the flowing phase in the absence of any criticality at the fluidization transition.

Finally we discuss what happens if the frequency of the driving force becomes distributed, instead of a single monochromatic frequency $\omega = 2\pi/820\tau_0$. Assuming the driving frequency for each particle is drawn from a flat distribution over the interval $[\omega - \frac{\Delta\omega}{2}, \omega + \frac{\Delta\omega}{2}]$, we discover that, at steady state, the long-time dynamics becomes diffusive for all values of a (see Sec. I in the SM for more details). From these long-time dynamics, we plot the inverse diffusion constant D^{-1} as a function of activity a in Fig. 3(d) for different frequency bandwidths $\Delta\omega$. We observe a clear discontinuous transition from a slow liquid ($D \sim$ small) for $a < a_c$ to a fast liquid ($D \sim$ large) for $a > a_c$. The values of D in the fast liquid phase are not strongly affected by $\Delta\omega$ and neither is the critical activity a_c. In the slow liquid phase, however, D becomes progressively slower as $\Delta\omega \to 0$ and finally the arrested-liquid transition is recovered in the limit of monochromatic frequency. Next, we also consider what happens when we prescribe a frequency distribution $P(\omega)$ with mean $2\pi/820\tau_0$ and variance $\Delta\omega^2$ to each particle's diameter $\sigma_i(t)$. We also find the discontinuous transition remains robust as long as $\Delta\omega$ is narrow enough (see Sec. II in the SM). Finally we consider a random but time-correlated noise in $\sigma_i(t)$ with correlation time $820\tau_0$ (Ornstein-Uhlenbeck noise; see Sec. III in the SM). In this case the discontinuous transition becomes a glass transition with diverging time scales and length scales.

In conclusion, we have introduced a microscopic model for active materials where local energy injection stems from active change of the particle sizes. We consider different types of size fluctuations (monochromatic frequency, mixed frequencies, and time-correlated noise). This model is inspired by experimental observations of volume fluctuations of cells in epithelial tissues [16,17]. For the first two cases, our model exhibits a discontinuous arrested (or nearly arrested) to liquid phase transition as the amplitude of self-deformation is increased. This transition is strikingly different from observations in self-propelled particles [25–27] in which continuous slowing down of several decades can be observed, accompanied by growing dynamic length scales, reminiscent of glassy dynamics in dense fluids [24]. It also differs markedly from the static transition discovered in the vertex model, which is akin to a continuous rigidity transition [21]. We propose that a better analogy is with the yielding transition in periodically driven soft amorphous solids, where irreversible rearrangements and particle diffusion result from applying a mechanical forcing above the yield stress. Evidence that yielding corresponds to a nonequilibrium dynamic first-order transition is mounting [34,35,37], the difference with our system being the scale at which the mechanical force is acting. Interestingly, when we consider time-correlated noise in the particle size fluctuations, this transition becomes a glass transition. This is as we expect because we no longer have a characteristic frequency in our system and thus we no longer have universality with the yielding transition of a periodically driven system. Instead, a better analogy to this type of forcing is that of self-propelled particles. It is interesting to test if fluidlike dynamics observed in biological tissues might fit into one of these three different kinds of size fluctuations.

We thank T. Kawasaki, M. E. Cates, and C. La Porta for discussion. The research leading to these results has received funding from the European Research Council under the European Unions Seventh Framework Programme (FP7/20072013)/ERC Grant Agreement No. 306845.

[1] M. C. Marchetti, J. F. Joanny, S. Ramaswamy, T. B. Liverpool, J. Prost, M. Rao, and R. A. Simha, Hydrodynamics of soft active matter, Rev. Mod. Phys. **85**, 1143 (2013).

[2] T. Vicsek and A. Zafeiris, Collective motion, Phys. Rep. **517**, 71 (2012).

[3] M. Poujade, E. Grasland-Mongrain, A. Hertzog, J. Jouanneau, P. Chavrier, B. Ladoux, A. Buguin, and P. Silberzan, Collective migration of an epithelial monolayer in response to a model wound, Proc. Natl. Acad. Sci. (USA) **104**, 15988 (2007).

[4] M. F. Copeland and D. B. Weibel, Bacterial swarming: A model system for studying dynamic self-assembly, Soft Matter **5**, 1174 (2008).

[5] V. Narayan, S. Ramaswamy, and N. Menon, Long-lived giant number fluctuations in a swarming granular nematic, Science **317**, 105 (2007).

[6] J. Deseigne, O. Dauchot, and H. Chaté, Collective Motion of Vibrated Polar Disks, Phys. Rev. Lett. **105**, 098001 (2010).

[7] I. Theurkauff, C. Cottin-Bizonne, J. Palacci, C. Ybert, and L. Bocquet, Dynamic Clustering in Active Colloidal Suspensions with Chemical Signaling, Phys. Rev. Lett. **108**, 268303 (2012).

[8] I. Buttinoni, J. Bialké, F. Kümmel, H. Löwen, C. Bechinger, and T. Speck, Dynamical Clustering and Phase Separation in Suspensions of Self-Propelled Colloidal Particles, Phys. Rev. Lett. **110**, 238301 (2013).

[9] L. Petitjean, M. Reffay, E. Grasland-Mongrain, M. Poujade, B. Ladoux, A. Buguin, and P. Silberzan, Velocity fields in a collectively migrating epithelium, Biophys. J. **98**, 1790 (2010).

[10] E. Mehes and T. Vicsek, Collective motion of cells: From experiments to models, Integr. Biol. **6**, 831 (2014).

[11] T. E. Angelini, E. Hannezo, X. Trepat, M. Marquez, J. J. Fredberg, and D. A. Weitz, Glass-like dynamics of collective cell migration, Proc. Natl. Acad. Sci. (USA) **108**, 4714 (2011).

[12] A. Puliafito, L. Hufnagel, P. Neveu, S. Streichan, A. Sigal, D. K. Fygenson, and B. I. Shraiman, Collective and single cell behavior in epithelial contact inhibition, Proc. Natl. Acad. Sci. (USA) **109**, 739 (2012).

[13] P. Rorth, Collective cell migration, Annu. Rev. Cell. Dev. Biol. **25**, 407 (2009).

[14] J. Ranft, M. Basan, J. Elgeti, J.-F. Joanny, J. Prost, and F. Julicher, Fluidization of tissues by cell division and apoptosis, Proc. Natl. Acad. Sci. (USA) **107**, 20863 (2010).

[15] S. M. Rafelski and J. A. Theriot, Crawling toward a unified model of cell motility: Spatial and temporal regulation of actin dynamics, Annu. Rev. Biochem. **73**, 209 (2004).

[16] S. M. Zehnder, M. Suaris, M. M. Bellaire, and T. E. Angelini, Cell volume fluctuations in MDCK monolayers, Biophys. J. **108**, 247 (2015).

[17] A. Taloni, E. Kardash, O. U. Salman, L. Truskinovsky, S. Zapperi, and C. A. M. La Porta, Volume Changes During Active Shape Fluctuations in Cells, Phys. Rev. Lett. **114**, 208101 (2015).

[18] S. K. Schnyder, Y. Tanaka, J. J. Molina, and R. Yamamoto, Collective motion of cells crawling on a substrate: Roles of cell shape and contact inhibition, arXiv:1606.07618.

[19] D. Bi, J. Lopez, J. Schwartz, and M. L. Manning, Energy barriers and cell migration in densely packed tissues, Soft Matter **10**, 1885 (2014).

[20] R. Farhadifar, J.-C. Roper, B. Aiguoy, S. Eaton, and F. Jülicher, The influence of cell mechanics, cell-cell interactions, and proliferation on epithelial packing, Curr. Biol. **17**, 2095 (2007).

[21] D. Bi, J. H. Lopez, J. M. Schwarz, and M. L. Manning, A density-independent rigidity transition in biological tissues, Nat. Phys. **11**, 1074 (2015).

[22] T. Vicsek, A. Czirok, E. Ben-Jacob, I. Cohen, and O. Shochet, Novel Type of Phase Transition in a System of Self-Driven Particles, Phys. Rev. Lett. **75**, 1226 (1995).

[23] S. Henkes, Y. Fily, and M. C. Marchetti, Active jamming: Self-propelled soft particles at high density, Phys. Rev. E **84**, 040301 (2011).

[24] L. Berthier and J. Kurchan, Non-equilibrium glass transitions in driven and active matter, Nat. Phys. **9**, 310 (2013).

[25] R. Ni, M. A. Cohen Stuart, and M. Dijkstra, Pushing the glass transition towards random close packing using self-propelled hard spheres, Nat. Commun. **4**, 2704 (2013).

[26] L. Berthier, Nonequilibrium Glassy Dynamics of Self-Propelled Hard Disks, Phys. Rev. Lett. **112**, 220602 (2014).

[27] E. Flenner, G. Szamel, and L. Berthier, The nonequilibrium glassy dynamics of self-propelled particles, Soft Matter **12**, 7136 (2016).

[28] S. R. Vedula, M. C. Leong, T. L. Lai, P. Hersen, A. J. Kabla, C. T. Lim and B. Ladoux, Emerging modes of collective cell migration induced by geometrical constraints, Proc. Natl. Acad. Sci. (USA) **109**, 12974 (2012).

[29] S. Garcia, E. Hannezo, J. Elgeti, J.-F. Joanny, P. Silberzan, and N. S. Gov, Physics of active jamming during collective cellular motion in a monolayer, Proc. Natl. Acad. Sci. (USA) **112**, 15314 (2015).

[30] N. Sepulveda, L. Petitjean, O. Cochet, E. Grasland-Mongrain, P. Silberzan, and V. Hakim, Collective cell motion in an epithelial sheet can be quantitatively described by a stochastic interacting particle Model, PLoS Comput. Biol. **9**, e1002944 (2013).

[31] D. Bonn, M. M. Denn, L. Berthier, T. Divoux, and S. Manneville, Yield stress materials in soft condensed matter, Rev. Mod. Phys. **89**, 035005 (2017).

[32] See Supplemental Material at http://link.aps.org/supplemental/10.1103/PhysRevE.96.050601 for a description of numerical simulations of various generalizations of the model.

[33] D. J. Durian, Foam Mechanics at the Bubble Scale, Phys. Rev. Lett. **75**, 4780 (1995).

[34] E. D. Knowlton, D. J. Pine, and L. Cipelletti, A microscopic view of the yielding transition in concentrated emulsions, Soft Matter **10**, 6931 (2014).

[35] T. Kawasaki and L. Berthier, Macroscopic yielding in jammed solids is accompanied by a non-equilibrium first-order transition in particle trajectories, Phys. Rev. E **94**, 022615 (2016).

[36] *Dynamical Heterogeneities in Glasses, Colloids and Granular Materials*, edited by L. Berthier, G. Biroli, J.-P. Bouchaud, L. Cipelletti, and W. van Saarloos (Oxford University Press, Oxford, 2011).

[37] P. Jaiswal, I. Procaccia, C. Rainone, and M. Singh, Mechanical Yield in Amorphous Solids: A First-Order Phase Transition, Phys. Rev. Lett. **116**, 085501 (2016).

Supplementary information: Other modes of particle's size fluctuations

Elsen Tjhung[1,2] and Ludovic Berthier[1,*]

[1] *Laboratoire Charles Coulomb, UMR 5221, CNRS and Université Montpellier, Montpellier 34095, France.*
[2] *Department of Applied Mathematics and Theoretical Physics, University of Cambridge, Cambridge CB3 0WA, UK*

(Dated: November 6, 2017)

The main ingredient in our active self-deforming particle model, is to allow the diameter of each particle to change with time t. Suppose we denote the diameter of particle i as $\sigma_i(t)$. We then specify a deterministic (or possibly stochastic) dynamics for $\sigma_i(t)$, separate from the dynamics for $\mathbf{r}_i(t)$ (or the particle's position). This will then break the microscopic detailed balance because we are injecting energy to the system locally. Our main result in the main text is to draw a connection between our active system to yielding transition in driven systems. This suggests that active and driven systems (although both are distinct classes of non-equilibrium systems) may share the same universality class at the fluidization transition.

In the main text, we consider a deterministic sinusoidal oscillation in the particle's diameter $\sigma_i(t)$ with a single driving frequency ω:

$$\sigma_i(t) = \sigma_i^0[1 + a\cos(\omega t + \psi_i)], \tag{1}$$

where ψ_i is a random phase difference for each particle and a is the activity parameter. The driving frequency $\omega = 2\pi/(820\tau_0)$ is the same for all particles and is taken to be much longer than the energy relaxation timescale τ_0. We then discover a discontinuous fluidization transition at some critical activity a_c.

In this Supplementary Information (SI), we explore three other possible modes of particle's size fluctuations. In the first part, we allow different driving frequencies ω_i for each particle i. In this case we find that the discontinuous transition remains robust, however, the fully arrested phase now becomes a nearly arrested liquid phase with very low diffusion constant. Thus we discover a novel route to a kind of liquid-liquid transition. In the second part, we consider a distribution of frequencies (with the same distribution for each particle). Here, we discover that the discontinuous fluidization transition discussed in the main text remains robust as long as the width of the distribution remains narrow enough, as expected. Finally in the last part, we consider a random size fluctuation with a coloured noise. In this case the discontinuous transition is destroyed and should become a non-equilibrium glass transition with forces that have a finite persistence times. But the model then becomes a physically different active system, where the very idea of particle reversibility is lost.

These additional results demonstrate that oscillatory driving (with some characteristic frequency) is necessary for the transition, thus, strengthening our hypothesis about similarity to the yielding transition in periodically driven systems.

I. MIXED FREQUENCIES FOR DIFFERENT PARTICLES

Instead of the same driving frequency ω for all particles, here, we shall consider a different driving frequency ω_i for each particle i:

$$\sigma_i(t) = \sigma_i^0[1 + a\cos(\omega_i t + \psi_i)] \tag{2}$$

where ω_i is taken randomly from a uniform distribution on the interval $[\omega_0 - \frac{\Delta\omega}{2}, \omega_0 + \frac{\Delta\omega}{2}]$. The average frequency, ω_0, is taken to be at $2\pi/(820\tau_0)$ or the same as the monochromatic frequency used in the main text, so that we can make a direct comparison with the results in the main text. Note that in this model, the global packing fraction is no longer strictly conserved, but it can fluctuate up to 0.3% (for $\Delta\omega/\omega_0 \lesssim 0.02\%$) around its initial packing fraction $\phi = 0.94$.

We perform additional simulations with $N = 1000$ for different values of activity a. Here, we consider two values of $\Delta\omega/\omega_0$: 0.002% and 0.02%. For each simulation, we start from an initially random configuration and measure the average displacement squared between time t and time $t + T$, where $T = 820\tau_0$, as defined in the main text:

$$d^2(t) = \frac{1}{N}\sum_{i=1}^{N} |\mathbf{r}_i(t+T) - \mathbf{r}_i(t)|^2 \tag{3}$$

* Email: ludovic.berthier@univ-montp2.fr

to check if the system has reached a steady state or not.

At steady state, we can then measure the mean squared displacement (MSD) as a function of delay time Δt:

$$\Delta r^2(\Delta t) = \left\langle \frac{1}{N}\sum_{i=1}^{N} |\mathbf{r}_i(\Delta t) - \mathbf{r}_i(0)|^2 \right\rangle \tag{4}$$

where the angle bracket indicate ensemble averaging over 80 independent simulations from different initial configurations but with the same a and $\Delta\omega/\omega_0$.

Fig. **??**(a) shows Δr^2 as a function of Δt for different a's at fixed $\Delta\omega/\omega_0 = 0.02\%$. The long time dynamics ($\Delta t \to \infty$) of Δr^2 appears to be diffusive for all values of activity a. Thus we can estimate the diffusion constant D as a function of activity a. Fig. **??**(a) also suggests a transition from a slowly-relaxing liquid ($D \sim$ small) to a fast-relaxing liquid ($D \sim$ large) at some critical activity $0.05 < a_c < 0.055$.

To quantify this more precisely, we plot the inverse diffusion constant D^{-1} as a function of a in Fig. **??**(b) for different values of frequency bandwidth $\Delta\omega/\omega_0$. D^{-1} is proportional to the relaxation timescale of the liquid phase. Here we see that D jumps discontinuously at the critical activity $a_c \simeq 0.05$. Thus we demonstrate that the discontinuous phase transition remains robust with respect to mixed driving frequencies (as long as the frequency bandwidth is narrow enough). We also discover that the arrested phase (when the driving is fully monochromatic) is now replaced by a liquid phase with extremely low diffsuion constant (for $a < a_c$), which is characterised by a relatively small diffusion constant D (the particles have moved less than one particle diameter after 1000 cycles!). In the limit $\Delta\omega \to 0$, or approaching the monochromatic frequency limit, the relaxation timescale for the slow liquid becomes longer and longer and eventually recovers the arrested phase described in the main text. This novel liquid-liquid transition has been observed in some equilibrium systems, but this is the first example where it has been observed in active systems.

Fig. **??**(c) shows the autocorrelation function (see main text for definition) of the steady state liquid phase as a function of activity a at fixed $\Delta\omega/\omega_0 = 0.02\%$. This also indicates a liquid-liquid transition at critical activity a_c. It might be interesting in the future to explore if similar liquid-liquid transition may also be observed in active self-deforming systems such as tissues as well as in periodically sheared systems.

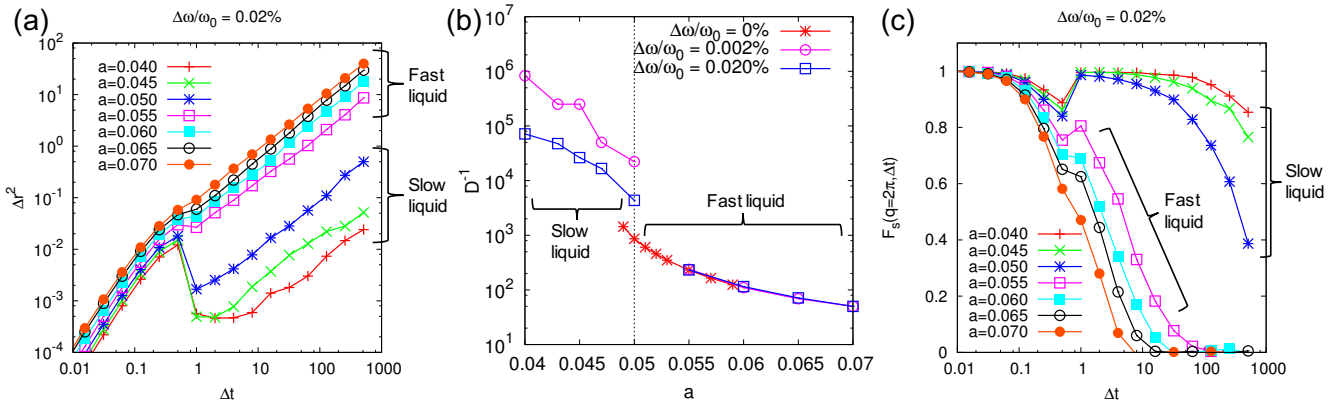

FIG. 1. (a) shows the steady state mean squared displacement Δr^2 as a function of delay time Δt for different activities a's at fixed $\Delta\omega/\omega_0 = 0.02\%$. (b) shows the inverse diffusion constant D^{-1} as a function activity a for different frequency bandwidth $\Delta\omega/\omega_0 = 0\%, 0.002\%$, and 0.02% (c) shows the autocorrelation function $F_s(q, \Delta t)$ as a function of delay time Δt at fixed $\Delta\omega/\omega_0 = 0.02\%$.

II. PRESCRIBING A FREQUENCY SPECTRUM IN EACH PARTICLE'S SIZE FLUCTUATION

In the second part, we now prescribe some frequency distribution $P(\omega)$ for each particle i (all particles having the same distribution $P(\omega)$, which is quite different from the part I). The size fluctuation of particle i can then be written as a Fourier transform of $P(\omega)$:

$$\frac{\sigma_i(t) - \sigma_i^0}{a\sigma_i^0} = \int d\omega\, P(\omega) e^{i(\omega t + \psi_i)} \tag{5}$$

(only the real part of the complex number is considered). In the case of monochromatic driving frequency: $P(\omega) = \delta(\omega - \omega_0)$, we will then recover the monochromatic sinusoidal fluctuation discussed in the main text:

$$\frac{\sigma_i(t) - \sigma_i^0}{a\sigma_i^0} = e^{i(\omega_0 t + \psi_i)} \tag{6}$$

where $\omega_0 = 2\pi/(820\tau_0)$.

Now let us consider, instead, a frequency spectrum centred around ω_0 with a width $\Delta\omega$. Without loss of generality, we can assume $P(\omega)$ to be Gaussian:

$$P(\omega) = \frac{1}{\sqrt{2\pi\Delta\omega^2}} e^{-\frac{(\omega-\omega_0)^2}{2\Delta\omega^2}}. \tag{7}$$

Substituting Eq. (**??**) to Eq. (**??**), we obtain the size fluctuation for particle i:

$$\frac{\sigma_i(t) - \sigma_i^0}{a\sigma_i^0} = e^{-\frac{\Delta\omega^2}{2}t^2} \cos(\omega_0 t + \psi_i). \tag{8}$$

Thus the particle's size still oscillates sinusoidally with frequency ω_0 like in the main text except that the oscillation now decays exponentially due to the prefactor $e^{-\frac{\Delta\omega^2}{2}t^2}$.

Consequently if the width of the frequency spectrum $\Delta\omega$ is narrow enough, the oscillation decays much longer than the observation time and we expect the results obtained in the main text to remain unchanged. To estimate the maximum value of $\Delta\omega$, we note that the decay timescale in the particle's size oscillation is of order $\sim 1/\Delta\omega$. In the main text, the longest relaxation time scale is given by τ_α at the critical value a_c, which is of order $\sim 10^2$ in units of periods (or $2\pi/\omega_0$). Thus the we require the frequency bandwidth to be less than: $\Delta\omega/\omega_0 \lesssim 0.01 = 1\%$. It should also be remarked that, in principle, it is possible to have a frequency-dependent phase difference $\psi_i(\omega)$, in which case, the situation may be similar to one described below.

III. RANDOM SIZE FLUCTUATION WITH COLOURED NOISE

Finally, we consider a random size fluctuation of particles' diameters as follow:

$$\sigma_i(t) = \sigma_i^0(1 + f_i(t)) \tag{9}$$

where $f_i(t)$ is an Ornstein-Uhlenbeck process satisfying:

$$\dot{f}_i = -\frac{1}{T} f_i + \sqrt{\frac{2}{T}} a\eta_i(t) \tag{10}$$

with T as the relaxation timescale and a as the noise strength. Here, a corresponds roughly to activity in the oscillatory driving model. $\eta_i(t)$ is a Gaussian random noise with zero mean and unit variance. $f_i(t)$ is then effectively a coloured noise with zero mean and variance:

$$\langle f_i(t) f_j(t') \rangle = \delta_{ij} a^2 e^{-|t-t'|/T}. \tag{11}$$

Eq. (**??**) can be solved numerically as follows:

$$f_i(t + \Delta t) = f_i(t) - \Delta t \frac{1}{T} f_i(t) + \sqrt{\frac{2\Delta t}{T}} a\eta_i(t). \tag{12}$$

Fig. **??** shows the typical time evolution of one particle's diameter as a function of time t for different relaxation times T's and activities a's.

We now perform simulations with $N = 4000$ for different values of activity a. Here we fix T to be $820\tau_0$ to compare with the results of the main text. Again we measure $d^2(t)$ to check if the system has reached a steady state or not. At steady state, we can then measure the MSD, Δr^2 as a function of delay time Δt as before. The result is plotted in Fig. **??**(a). As can be seen from the MSD, the long time dynamics of MSD becomes more sub-diffusive for decreasing a. This is reminiscent to glass transition with the glass transition point close to $a = 0$. Similarly the auto-correlation function (Fig. **??**(b)) indicates a diverging relaxation timescale as $a \to 0$.

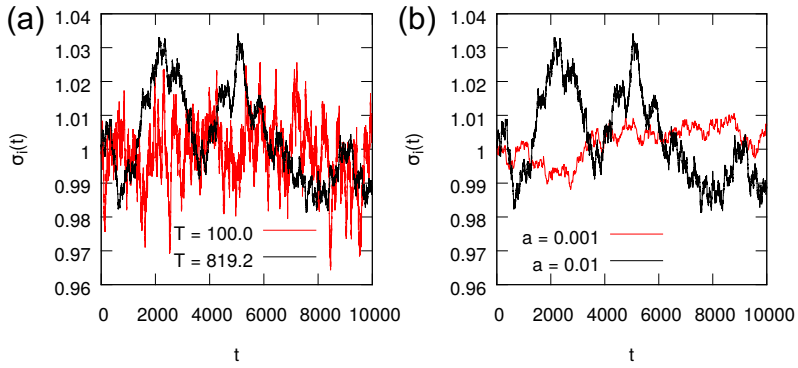

FIG. 2. (a) shows the time evolution of one particle's diameter for two different relaxation times T's (a is fixed to be 0.01). (b) shows the time evolution of one particle's diameter for two different activities a's (T is fixed to be $820\tau_0$).

Thus by switching the dynamics for $\sigma_i(t)$ from oscillatory to noisy, we destroy completely the discontinuous phase transitions. This is as we expect because in yielding transition, the phase transition coincides with the breakdown of microscopic reversibility. In order for the notion of microscopic reversibility to be meaningful, we require some forms of oscillatory driving with some characteristic frequency. In the Ornstein-Uhlenbeck type of size fluctuation, we no longer have this periodicity and thus the phase transition is destroyed and instead the physics becomes similar to the one of self-propelled particles where active forces are characterized by finite persistence times. This situation has been studied before and falls into a different universality class. Overall, these results strengthen our hypothesis for the active yielding transition.

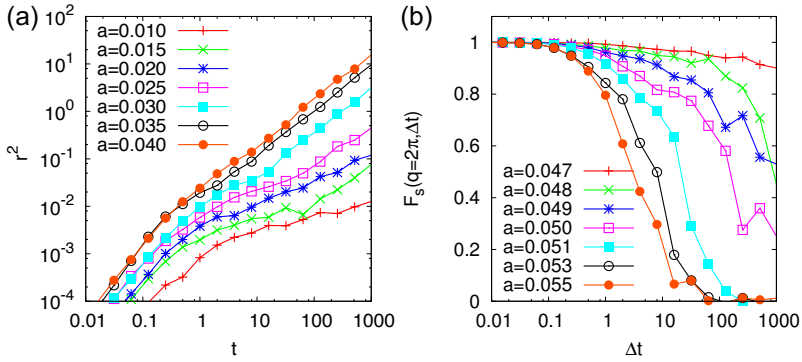

FIG. 3. (a) shows the mean squared displacement (MSD) Δr^2 as a function of delay time Δt for different activities a's. (b) shows the autocorrelation function $F_s(q, \Delta t)$ as a function of delay time Δt.

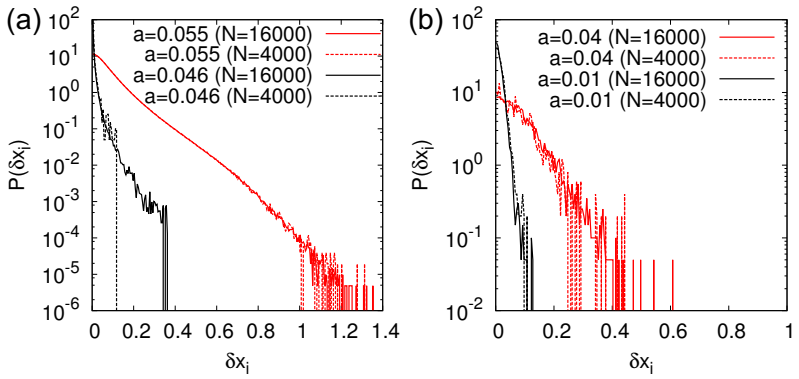

FIG. 4. shows the distribution of particles' displacements δx_i at steady state (see main text for definition) for different system sizes for (a) cyclic swelling model with monochromatic frequency as in the main text, and (b) random swelling model with coloured noise.